In: AIAA SciTech Forum 2023, 23-27 January 2023, National Harbor, Maryland.
DOI: 10.2514/6.2023-0837

Set-Based Design Space Exploration to Investigate the Effect of Energy Storage Durability on the Energy Management Strategy of a Hybrid-Electric Aircraft

Andrea Spinelli*, Gustavo P. Krupa† and Timoleon Kipouros‡
Cranfield University School of Aerospace Transport and Manufacturing, Cranfield, MK43 0AL, UK

To investigate the key enabling technologies for hybrid-electric regional aircraft, several assumptions about the maturity and required level of technology are necessary. Within the EU-funded project FutPrint50, a decision-making framework based on Set-Based Design principles is being developed to address these uncertainties arising from operational requirements and technological feasibility levels. The methodology has been applied to study the effects of the energy storage durability and technology level on the energy management strategies of a regional hybrid-electric aircraft. Results highlight the key role of battery energy density on the durability of the battery pack and the viability of the hybrid-electric aircraft concept. Additionally, the trade-off between zero-day environmental compatibility and battery lifetime is identified alongside its causing mechanism. Optimal energy management strategies are suggested in light of this new information. Finally, statistical data of cell energy density is used to estimate the most probable year of feasibility of hybrid-electric propulsion for regional aircraft.

I. Nomenclature

C_t	=	Battery Cell equivalent Capacitance [Farad]
DOH	=	Degree of Hybridization
DOD	=	Battery Depth of Discharge
E_{cell}	=	Energy capacity of the cell [Ah]
$e_{battery}$	=	Energy density of the battery pack [Wh/kg]
$E_{mission}$	=	Total charge required to fly the mission [Ah]
F_{flow}	=	Gas Turbine Fuel Flow [kg/s]
h	=	Degree of Hybridization (as defined in the EMS)
I_{cell}	=	Current in the cell [A]
M_{TO}	=	Take-Off Mass [kg]
M_f	=	Fuel Mass [kg]
M_b	=	Battery Pack Mass [kg]
N_{series}	=	Number of cells in series per bar
$N_{modules}$	=	Number of modules in parallel in the pack
P_B	=	Power required by the battery pack
P_{GT}	=	Power required by the gas turbine
P_{sat}	=	Minimum probability to satisfy a constraint
R_0	=	Cell Internal Resistance [Ohm]
R_t	=	RC Transient Resistance [Ohm]
U_{cell}	=	Cell Voltage [V]
V_c	=	Cell Capacitance Voltage [V]
V_{OC}	=	Cell Open-circuit Voltage [V]
V_{sys}	=	System Nominal Voltage [V]
Δ_{DOH}	=	Slope of the linear Degree of Hybridization function

*Ph.D. Candidate, Centre for Propulsion and Thermal Power, andrea.spinelli@cranfield.ac.uk, AIAA Member
†Research Fellow, Centre for Propulsion and Thermal Power, g.krupa@cranfield.ac.uk
‡Senior Lecturer, Centre for Propulsion and Thermal Power, t.kipouros@cranfield.ac.uk, AIAA Member

Published by AIAA. This is the Author Accepted Manuscript issued with: Creative Commons Attribution Non-Commercial License (CC:BY:NC 4.0).
The final published version (version of record) is available online at DOI:10.2514/6.2023-0837. Please refer to any applicable publisher terms of use.

η_E	=	Efficiency of the electrical powertrain (Propeller-to-Battery)
η_{GT}	=	Efficiency of the thermal powertrain (Propeller-to-Gas Turbine)
μ_{DOH}	=	Average Degree of Hybridization of a linear function

II. Introduction

SINCE the beginning of the 21st century, aeronautical research has been focused on reducing its global footprint on the environment by reducing emissions. Recent advancements in the development of battery technology and electrified ground vehicles spurred the investigation and research into the electrification of aircraft propulsion. One domain of research consists in introducing electric power in synergy with the internal combustion engines (ICE), in a hybrid propulsion system. The general idea is to maintain the ICEs in the ideal operating condition when flying in high power conditions [1]. Finding the correct amount of electric power to achieve this ideal condition is the aim of the Energy Management System (EMS).

Both system parameters and the flightpath concur to the identification of the optimal EMS. Many authors in the literature have explored the interaction between the flightpath and EMS, both in a local optimization and global optimization fashion with a fixed Hybrid Electric Propulsion System (HEPS) configuration [2–4]. On the other hand, there has been little published work regarding the interaction between the hybrid propulsion system and the optimal EMS for a design mission, such as the role of the EMS in battery aging. Currently, few studies have been published targeting this specific problem but limited to the Urban Air Mobility (UAM) sector [5, 6]. This gap falls within the scope of the FUTPRINT50 project [7], which aims to identify and assess the role of the key technologies required for the successful implementation of hybrid-electric propulsion for regional turboprop airplanes [8–10]. Alongside this technical goal, the project aims to develop a design space exploration and optimization framework that takes into consideration the uncertainty of a new design and provides multiple alternatives in deciding which concept to pursue for a given set of top level requirements. This objective is aligned with the general research suggestions proposed by NASA in their Vision 2040 program for multidisciplinary optimization, Uncertainty Quantification (UQ), and decision-making frameworks [11]. In particular, recent frameworks applied on hybrid-electric aircraft designs focus more on the simulation and optimization of the design, without evaluating the impact of technological uncertainty [12–14]. The reason is due to the difficulty of predicting the interval of values as no hybrid-electric aircraft has reached production yet. Di Bianchi [15] and Guenov [16] presented methods, respectively based on reliability-based optimization and margin value method, for managing technological uncertainty in future concepts.

This framework is being implemented by introducing Set-Based Design elements in Multi-disciplinary Optimization and Uncertainty-based Optimization. In previous work [17], the methodology has been demonstrated through the study of the trade-off between environmental compatibility, as NO_x emissions, and aircraft desirability, in the form of fuel consumption. A simple constant efficiency battery model was used to capture the effect of the EMS over the mass of the energy sources (batteries and fuel) required to fly the specified mission.

We extend the study by integrating a more detailed battery pack model, which captures the efficiency of the cell as it discharges, as well as its degradation after several cycles. The scope is to investigate the effects of the durability of the energy storage system to the EMS, as well as control the critical properties of the behavior of this system. The presented test case aims to find those EMS which achieve a balance between reduction of fuel consumption, aircraft emissions, CO_2 and NO_x, and battery degradation after one year of usage. Finally, this analysis is carried out with different values of battery energy density $e_{battery}$, to assess the different technological scenarios, including a probabilistic estimation of the earliest year of availability.

III. Methodology

A. Design Space Exploration Methodology

The design space exploration methodology used, called Probabilistic Design and Optimization (P-DOPT), has been developed by combining Set-Based Design principles with Multi-objective Optimization [18]. In Set-Based Design, it is straightforward to generate configurations for systems that can be described by discrete design parameters, such as subsystems or components. The initial step is to tabulate the identified design system parameters along with their possible options. These parameters are recombined for each new alternative configuration and evaluated according to a predefined set of performance metrics. The configurations that do not satisfy the design requirements are discarded and the remaining ones are stored for future use, and the process continues until a desirable configuration emerges [19].

The conventional engineering design method is iterative and traditionally follows the classical V-model [20]. In Set-Based Design, the conventional design approach may be referred collectively as "point-based methods", where few configurations and alternatives are evaluated in the conceptual design phase. Then, the subsystems are developed in the preliminary design. The design is frozen and detail design work continues. Often this design process leads to the paradoxical situation of needing to establish requirements early.

The adoption of Set-Based Design concepts in an engineering design project can change the way engineers interact, and how novel aircraft products are designed. The early analysis of multiple configurations and their subsequent pruning allows the designers to build a knowledge base of how the model responds and maintain a range of alternative configurations in case the requirements change. However, the flexibility brought by set-based design adds uncertainty and organization pressure in the process since the consideration of multiple options may yield a delay in the design pipeline unless the narrowing is done aggressively [21].

The design space exploration methodology was developed to evaluate multiple configurations of the design problem and estimate how many of these satisfy the requirements specified by the user. This process is carried out by constructing a probabilistic surrogate model whose response can calculate the probability of a design subspace of satisfying the requirements. This has been shown to reduce significantly the areas of design space to be later searched by the optimization algorithm, cutting computing time up to 80% [22]. Figure 1 presents a breakdown of the process. The proposed framework can be used in combination with parallel studies to support activities of technology and product forecasting. In the particular case of feasibility scenarios concerning hybrid-electric propulsion, the battery pack energy density is a figure of merit of utmost importance. Section V.F presents an example of a such study.

By estimating the probability of achieving the expected technological requirements, the designer can use this information in the proposed approach to investigate the design space exploration of future technology scenarios. More details on the methodology can be found in [17].

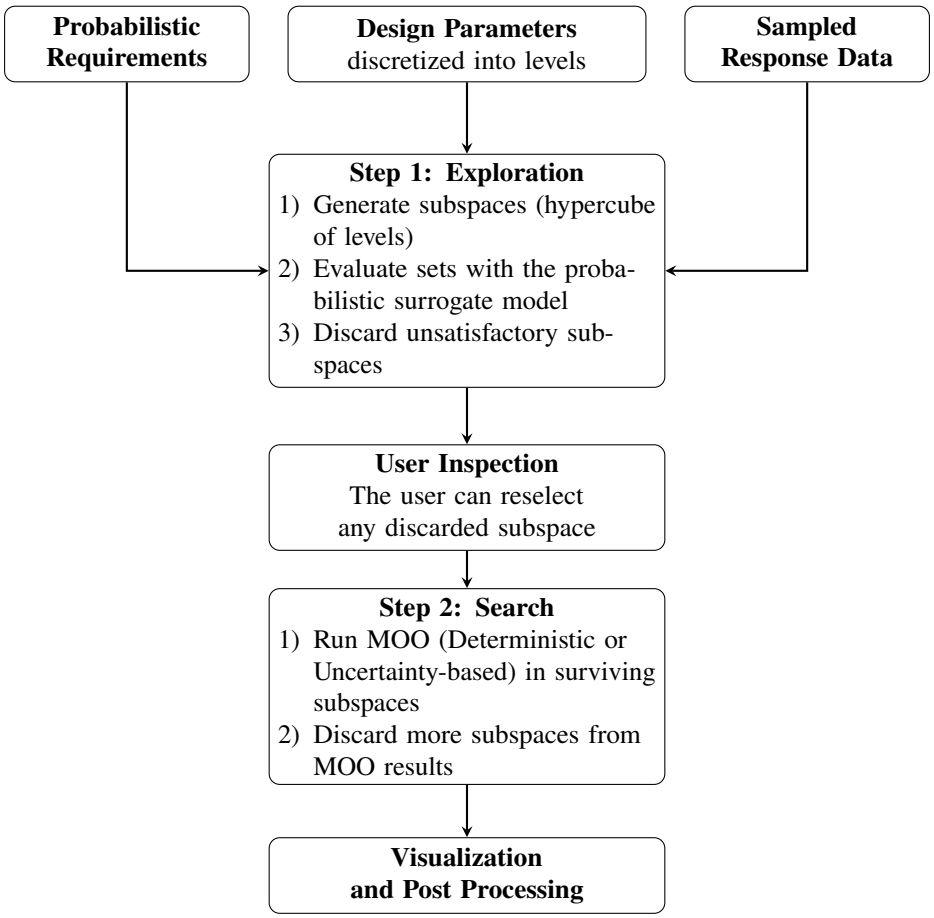

Fig. 1 Methodology Flowchart.

It is important to highlight that the multi-objective optimization (MOO) performed can be either deterministic or uncertainty-based. An uncertainty-based MOO is grounded on the fact that uncertainty is all-pervasive in engineering design and analysis, in the measurements taken and, also in the assumptions that engineering and mathematical models rely on. As an example of how the inclusion of uncertainties is desirable, one may consider the problem of investigating the overall system uncertainty regarding the energy density of the cells and the efficiencies of the electrical components projected for the year 2035 [23]. This uncertainty may result from the manufacturing processes and the aging of any system, which introduces deviations from the specifications and the operating conditions always vary from the nominal ones. In such cases, one can model nominal parameters with probability distributions that are capable of taking into account both aleatory and epistemic uncertainties [24]. Under this perspective, these parameters are called Interesting Quantities (IQ) and are used to quantify the response to uncertainty parameters and design variables.

As a general rule, problems that deem robustness and reliability more significant than nominal results employ optimization under uncertainties methods. They can find an optimum by constructing an uncertainty-based counterpart of the original objective function. Thus, the use of uncertainty-based methods makes it possible to address the performance, feasibility, and reliability during the early design space exploration, which effectively leads to a robust and reliable understanding of the system under design and its impact on a downstream system such as the hybrid electric propulsion one. This approach inevitably leads to results that consist of multidimensional data. The visualization of multidimensional data produced is carried out with the aid of parallel coordinates diagrams. Combined with scatter plots, this type of visualization can help the designer to understand the relationships between input parameters, responses, and constraints [25].

B. Aircraft and Propulsion Model

The selected aircraft is a 50-seater turboprop obtained from retrofitting an ATR-72, where part of the payload mass has been replaced by the battery pack mass. Mass and aerodynamics data have been extracted from information available on the ATR 72-600 [26, 27]. These are presented in Table 1. The operating empty mass (OEM) figure is kept constant as it is assumed the mass of the electrical equipment that is not the battery pack has a marginal contribution to the total take-off mass increment. Therefore, it has been ignored since this high level study does not consider the sizing of these components. Furthermore, a major assumption is the OEM does not change with the battery pack mass, and structural resizing is neglected, therefore the maximum take-off weight of the reference ATR-72 is imposed as a constraint.

Maximum Take-Off Mass	23,000 kg	Payload Mass	5000 kg
Operating Empty Mass	11,550 kg	Gearbox Efficiency	0.99
L/D Climbout	10.5	Propeller Efficiency (Take-Off)	0.64
L/D Climb/Descent	16	Propeller Efficiency (Climb)	0.73
L/D Cruise	14.5	Propeller Efficiency (Cruise)	0.86
L/D Final	7.5	Propeller Efficiency (Other)	0.8

Table 1 Aircraft Properties.

The propulsion system is a mechanically integrated parallel hybrid propulsion unit, whose power is provided by a gas turbine and an electric motor, as shown in Figure 2.

The gas turbine is a thermodynamically equivalent model of the Pratt & Whitney Canada PW127 engine, whose performance data has been generated using the in-house code TURBOMATCH[28, 29]. It is assumed that the electric propulsion component is introduced as a retrofit to the aircraft, hence the baseline gas turbine is not resized for hybridization. Constant propeller efficiency has been assumed for different mission phases. The NO_x emissions model is based on the Boeing FuelFlow2 method [30], which is a simplified P3T3 method useful when manufacturer data is not available. The data required to model the turboprop emission indice EI_{NO_x} was collected from Filippone and Bojdo [31].

Electric motors, power electronics, and cabling are modeled with a single constant efficiency parameter, whose values have been adopted from [23]. The battery pack is modeled with a Thevenin equivalent circuit, as explained in III.C. The TMS is assumed to keep the battery temperature at $25°C$. A TMS will be designed and modeled and its dynamic off-design performance impact on the battery temperature and its operation will be investigated in the final paper.

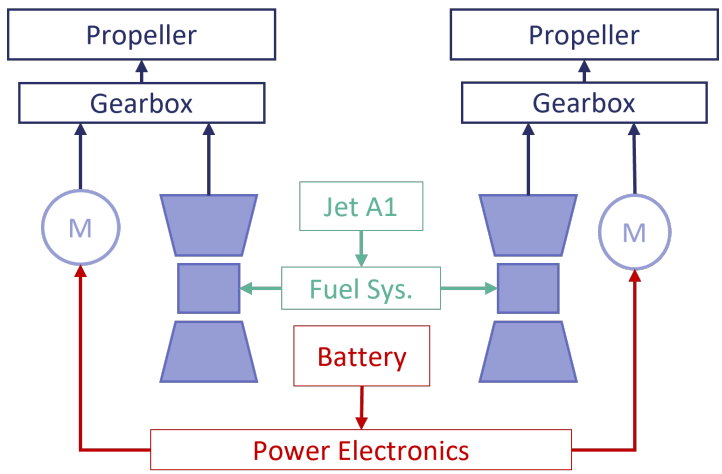

Fig. 2 Propulsion System Architecture.

Electric Motor Efficiency	0.98
Power Electronics Efficiency	0.985
Cable Distribution Efficiency (Circuit Breakers)	0.996
Packaging Factor (Pack-to-Cell Mass Ratio)	1.5
Cell Total Capacity [Ah]	7
Cell Nominal Voltage [V]	3.7
Cell Mass [kg]	0.0518

Table 2 Electric propulsion system parameters.

C. Battery Model

To capture in detail the efficiency of the battery pack and its behavior when subjected to different energy management strategies, a Thevenin equivalent circuit model was developed. Equations 1 describe the behavior of the single battery cell. Reference [32] provided the equations for the behavior of the lumped components V_{OC}, R_0, C_t, R_t under different values of depth of discharge DOD, while the properties of the cell are presented in Table 2. The cell mass is calculated to match the selected battery pack energy density. The Pack-to-Cell mass ratio is 1.5, taken from the Battery model of the NASA X-57 Maxwell [33]. Nonetheless, this value is optimistic as safety and certification requirements would increase the insert mass of the pack [34].

$$\begin{aligned}
&\frac{dV_C}{dt} = \frac{I_{cell}(t)}{C_t} - \frac{V_C(t)}{R_t\, C_t} \\
&\frac{dDOD}{dt} = \frac{I_{cell}(t)}{E_{cell}} \\
&U_{cell} = V_{OC} - V_t - I_{cell}\, R_0 \\
&P_B = U_{cell}\, I_{cell}\ \ (N_{series} \times N_{modules})
\end{aligned} \tag{1}$$

Power provided to the cell is calculated by dividing the required battery power at the pack terminals. The pack is composed of groups of cells in series called modules, which are arranged in parallel to each other to meet the required capacity. The battery pack sizing procedure is as follows:

1) Calculate the number of cells in series for each bar to meet the nominal system voltage: $N_{series} = \frac{V_{sys}}{V_{cell}}$
2) Increment the charge required to fly the mission by a guessed factor k: $E_{total} = k \times E_{mission}$
3) Calculate the number of modules to meet the required capacity: $N_{modules} = \frac{E_{total}}{E_{cell}}$
4) Simulate the cell discharge by solving eq. 1 after dividing the pack power by the total number of cells

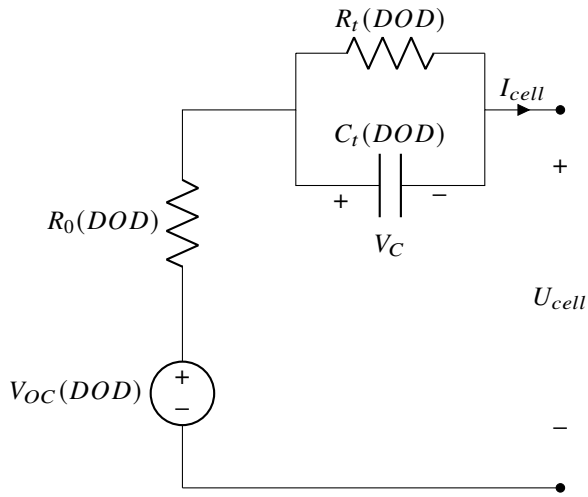

Fig. 3 Thevenin Electric Model for a Battery Cell.

$P_{cell} = \frac{P_B}{N_{series} N_{modules}}$

5) Repeat steps 2-4 by changing k, until the pack depth of discharge matches the target of 80%.
6) Calculate the total mass of the pack by multiplying the number of cells by the cell mass. This value is then incremented by the packaging factor to account for the battery pack mass overhead.

With the battery pack properly sized, the circuit model is run to evaluate the efficiency of the battery pack and its discharge characteristics.

D. Battery Aging Model

The holistic aging model developed in [35] was adopted to model the fade of the energy and capacity of the cell and the growth of its internal resistance, as it is put into operational use. Results from the equivalent circuit model of III.C (current, voltage, and depth of discharge) allow to estimate the degradation of the lumped circuit parameters after one cycle. Cell temperature is also present as input. Nevertheless, for this study, it is assumed the thermal management system maintains it in the ideal range.

The simulation of the battery pack aging is performed by running the mission analysis and updating the cell parameters after a certain amount of time has passed. This study evaluates the battery pack performance after one year of operations, assuming 2 flights per day, 7 days per week. A 5 days time-step was selected as an adequate trade-off between computational cost and error.

E. Mission Analysis Method

Figure 4 presents the procedure used to find the burned fuel mass and the battery pack mass for the specified mission. After an initial guess of the fuel mass M_f and the battery pack mass M_b, the mission take-off mass M_{TO} is calculated and iteratively updated until both fuel and battery pack masses converge. Two nested loops are used, the innermost for M_f and the outmost for M_b.

The calculation is performed by splitting the entire mission into small parts, and for each of them calculating the power required to fly each phase, using the altitude h, velocity V and climb rate V_z prescribed by the mission. This power is then split between the two powertrains with the specified degree of hybridization DOH, and chain efficiencies are applied to calculate the power required by the gas turbine P_{GT} and by the battery pack P_B. The burned fuel mass is calculated by multiplying the current fuel flow F_{flow} of the gas turbine by the elapsed time, and summed over all the mission phases. Once the fuel mass is converged, the total charge is calculated and used to size the battery pack with the procedure explained in III.C. After sizing the battery pack, the degraded condition is evaluated. The procedure simulates one year of operational life, updating the energy capacity and internal resistance after every 5 days. At each step the original energy management DOH is scaled proportionally, without changing its topology, to avoid the battery going above the 80% depth of discharge. Since the capacity of the cells reduce as it ages, more fuel is required to carry

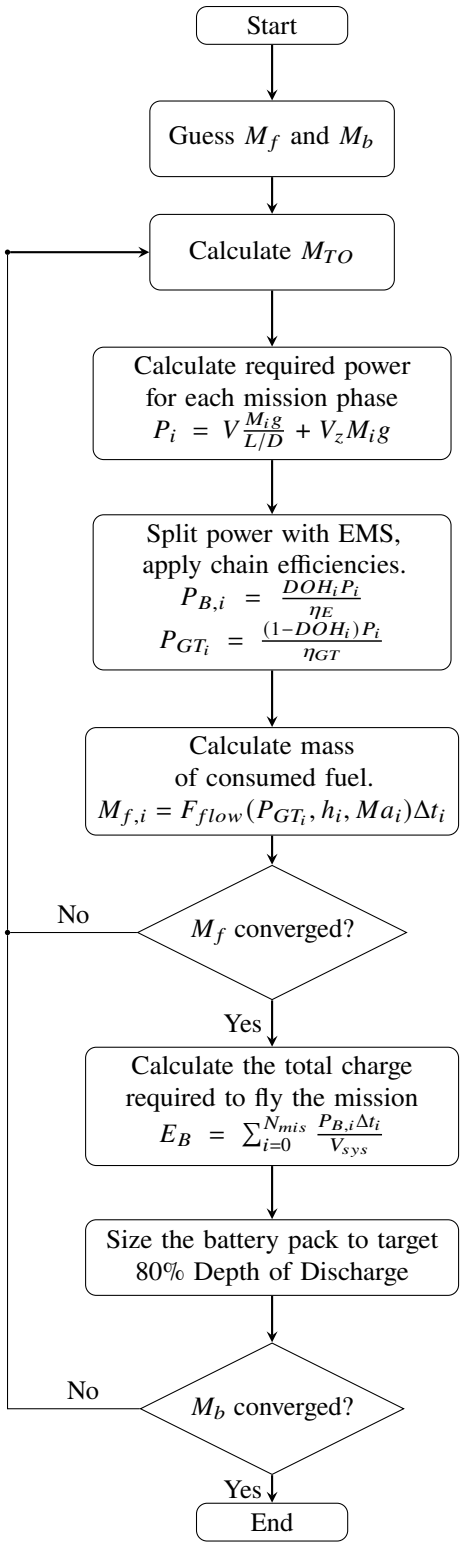

Fig. 4 Mission Analysis Method Flowchart.

out the same mission, hence it is reasonable to adopt as a representative variable for battery aging the ratio between the original fuel consumption and the fuel consumption after one year of use (Eq. 2).

$$r_{degr} = \frac{M_{fuel,\,1\,year\,use}}{M_{fuel,\,fresh\,battery}} \tag{2}$$

F. Design Mission and Energy Management profile

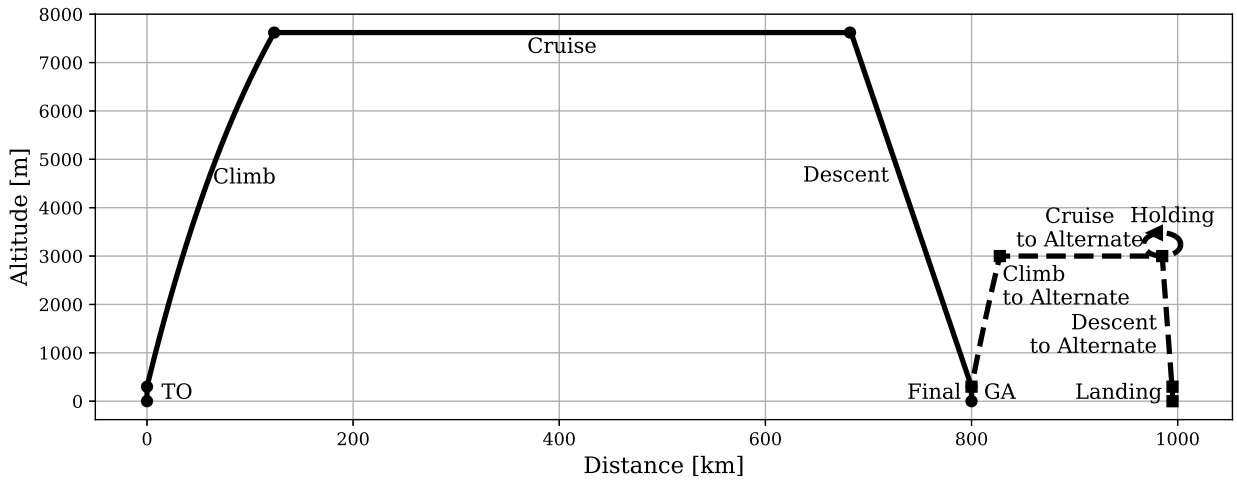

Fig. 5 Mission profile.

The selected mission profile is shown in Figure 5, which has been adopted by the FutPrint50 [8] project as a maximum range design mission, including a flight to an alternate airport to account for fuel reserves. The main flight stage is 432 nm (800 km) and the alternate stage of 51 nm (95 km) with a 30-minute holding pattern. The average climb rate is 996 ft/min (5.059 m/s), while the cruise speed is 268 kt (137.78 m/s).

It is assumed that the aircraft would have exhausted its energy reserves (fuel and batteries) at the end of the entire flight. Electric power use is restricted to the climb and cruise phases of the main portion of the mission.

Energy management strategies are defined as a continuous piecewise linear DOH function over the entire mission, with values ranging from 0 to 1 (Fig. 6), as detailed in Ref. [17]. These parameters allow for a flexible definition of the shape of the EMS over each phase. In total, 4 parameters describe a complete energy management strategy for a full mission analysis.

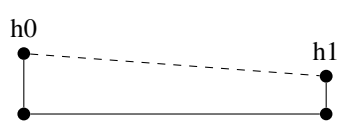

Fig. 6 Linear Energy management strategy adopted for this study.

IV. Test Case

The design space exploration test case is formulated as an optimization problem, shown in Eq. 3. For this study, we consider linear energy management segments, applied to the climb and cruise phases, and the energy density of the battery pack. Input values for the P-DOPT framework are presented in Table 3. The selected figures of merit are the total burned fuel during the mission M_f, the mass of the emitted NO_x, and the ratio of the burned fuel mass after one year of operation over the original amount with a fresh battery pack.

$$
\begin{aligned}
&\text{given} && X = \{e_{battery}, h0_{cl},\ h1_{cl},\ h0_{cr},\ h1_{cr}\} \\
&\underset{X}{\text{minimize}} && M_{fuel},\ M_{NO_x},\ r_{degr} \\
&\text{subject to} && M_{TO} \leq 23000\,\text{kg}\ (P_{sat} \geq 0.5)
\end{aligned}
\tag{3}
$$

Parameter		Values
Pack Energy Density [Wh/kg]	$e_{battery}$	[350, 400, 450, 500, 550]
Start Climb DOH	$h0_{cl}$	(0,1) divided into 4 levels
End Climb DOH	$h1_{cl}$	(0,1) divided into 4 levels
Start Cruise DOH	$h0_{cr}$	(0,1) divided into 4 levels
End Cruise DOH	$h1_{cr}$	(0,1) divided into 4 levels

Table 3 Input Parameters.

This last objective is to study the system performance effects of aggressive hybridization when the battery pack is fresh. While it is not directly a battery pack parameter, it is an indicator of how much the capacity of the cell has degraded over one year of operation. Indeed, to meet the same 80% DOD target, the energy management system has to use more power from the gas turbine powertrain, leading to higher fuel consumption and higher emissions.

The take-off mass M_{TO} is constrained to the ATR-72 maximum take-off mass, and introduced as a probabilistic constraint to the exploration step, with a minimum satisfaction probability P_{sat} of 50%. Areas of the design space that fall below this threshold are discarded and not considered for optimization.

Results are compared to the baseline, which is the same ATR-72 model without electric propulsion and loaded with the same payload. Values for the baseline are presented in Table 4.

Take-Off Mass	17,792 kg
Burned Fuel	1242 kg
NO_x Emission	8.59 kg

Table 4 Baseline Quantities.

V. Results

Figure 7 presents the Pareto front solutions produced by the design space exploration framework. Three major results are clear from this graph. First, high $e_{battery}$ produces higher values of r_{degr} overall. However, when comparing equal values of fuel burn reduction, the battery ages slower when the specific energy is higher (Fig. 7a). As will be discussed later, this is caused by the mass of the cells and not the cell aging (Fig. 10). With more energy per unit of mass, fewer cells are required to achieve the same reduction in fuel consumption. The airplane is less heavy, hence when the capacity fades over time, the dead weight of the batteries has a smaller impact on fuel consumption. Instead, when all the mass available for batteries is used, the rate of degradation is higher because of the higher extra dead weight.

Secondly, the rate of degradation and the other two objectives compete, most evidently with the reduction of fuel consumption. This trade-off is important for airline operators, where the cost of fuel and the cost of battery maintenance would compete.

Finally, the results indicate that the pack energy density should be greater than 400 Wh/kg in order to reduce the emissions and fuel consumption above the baseline (Fig. 7b). This sets a technological requirement of a minimum 600 Wh/kg energy density for the individual cells, which will be achieved no earlier than the year 2040, as discussed in section V.F.

The following subsections explore the data in detail, analyzing the interaction between $e_{battery}$, r_{degr}, EMS, and the battery life alongside the performance of the aircraft compared to the baseline.

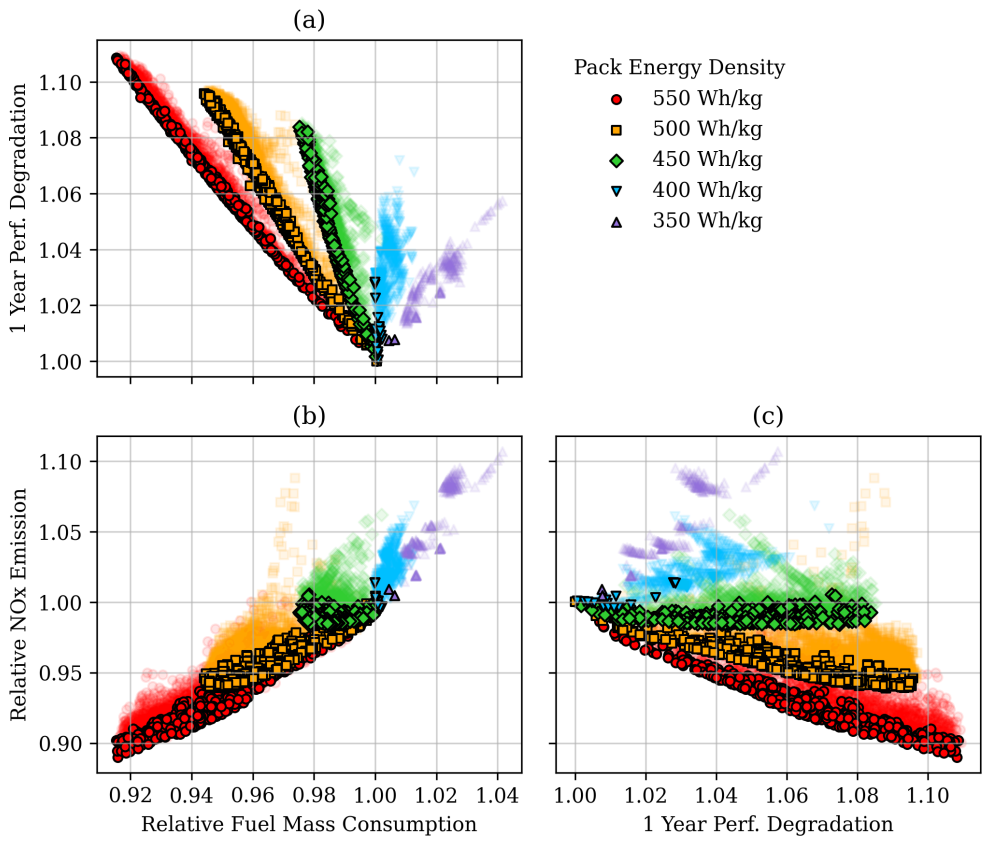

Fig. 7 Pareto front of the three objectives with different battery pack energy densities.

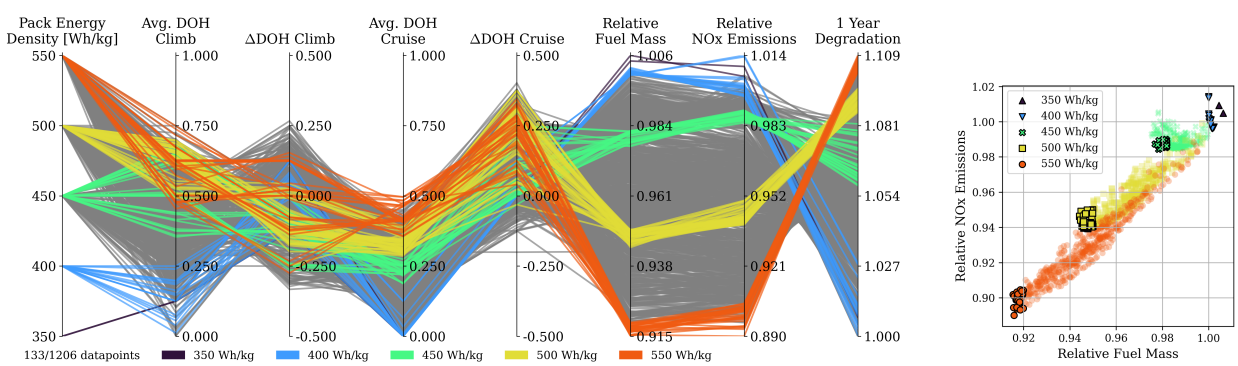

(a) Parallel coordinates with selections.

(b) Pareto front with selections.

Fig. 8 Effects of Battery Energy Density on the Energy Management Strategies.

A. Effects of $e_{battery}$ on Energy Management Strategies

Figure 8 presents the resulting optimal energy management strategies for each level of battery energy density. Since the strategies are all linear segments, the input variables have been decomposed into an average value, the segment midpoint, and discrepancy, the slope of the segment, as shown in Equation 4.

$$\begin{cases} \mu_{DOH} = \frac{h_1+h_0}{2} \\ \Delta DOH = \frac{h_1-h_0}{2} \end{cases} \tag{4}$$

Higher values of energy density allow for higher values of average DOH, both in climb and cruise. More of the flight power can be provided by the electrical source at the same maximum take-off mass limit. The climb segment is more hybridized than the cruise segment. Regarding the slope of the segments, the cruise phase presents a positive slope directly correlated with the energy density. On the other hand, the climb segment presents a negative slope with some exceptions, at the highest $e_{battery}$ of 550 Wh/kg. In conclusion, more specific energy in the battery pack enables more hybridization and more flexibility in the slope of the segments, owing to being able to store more electrical power onboard for the same amount of maximum take-off mass.

B. Effects of r_{degr} on Energy Management Strategies

Figure 9 presents for three different levels of battery energy density the effect of the degradation parameter r_{degr} over the other variables. Battery life was calculated as the number of days after which the electrified airplane matches the fuel consumption of the baseline conventional aircraft (see Fig. 10(a)). It is correlated with r_{degr}, where the battery lasts the longest with low degradation EMS. All three technological scenarios feature similar correlations between r_{degr} and the average values of DOH: the higher the electrical power demand, the faster the degradation of the cells. On the other hand, ΔDOH is concentrated around zero when r_{degr} is the lowest. It spreads without a specific trend at values of high degradation. It can be concluded that the average electrical power requirement drives the degradation of the cell, rather than the specific value over time.

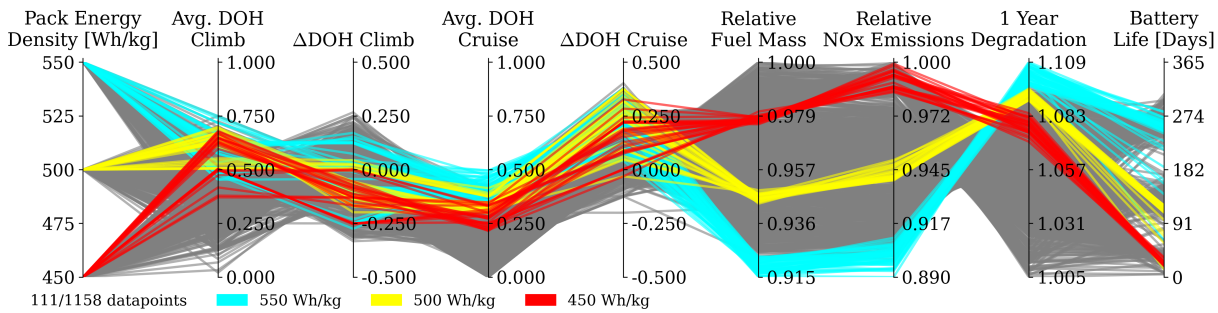

(a) High values of r_{degr}.

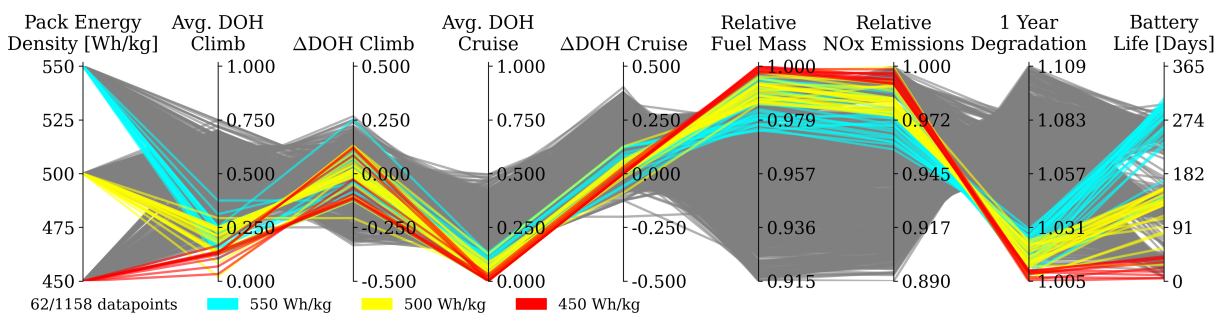

(b) Low values of r_{degr}.

Fig. 9 Effects of Degradation on the Energy Management Strategies.

C. Effects of $e_{battery}$ on r_{degr} and Battery Life

Six specific points, two per $e_{battery}$ value, were selected for analyzing the history of battery degradation over one year of operation. Each pair is composed of the designs with least fuel consumption at zero days and the highest battery life, as defined in the previous section V.B. Figure 10 presents these results on two scales: fuel consumption relative to the conventional baseline and relative to the day zero condition.

As shown in Fig. 10(a) the lifetime of the battery is greater with higher $e_{battery}$ and, respectively, the gap from the lowest degradation to the highest is larger for each case. In contrast, Fig. 10(b) shows that r_{degr} grows faster when $e_{battery}$ is greater and the degradation is high, the opposite is true when degradation is low. Despite all these differences,

the actual degradation of the cell (capacity fade and internal resistance growth) is identical for all six cases (Fig. 10(c) and 10(d)). Indeed, the parameters that would affect the cell degradation, such as the temperature, initial state of charge, and depth of discharge, are identical for all the cases. This would change if partially re-charging the airplane after one flight is introduced in the analysis, a scenario that has been suggested by the authors for regional aircraft operations [36]. More flights could be carried out per day, at the cost of using the battery from a partial state of charge, hastening the aging of the cells.

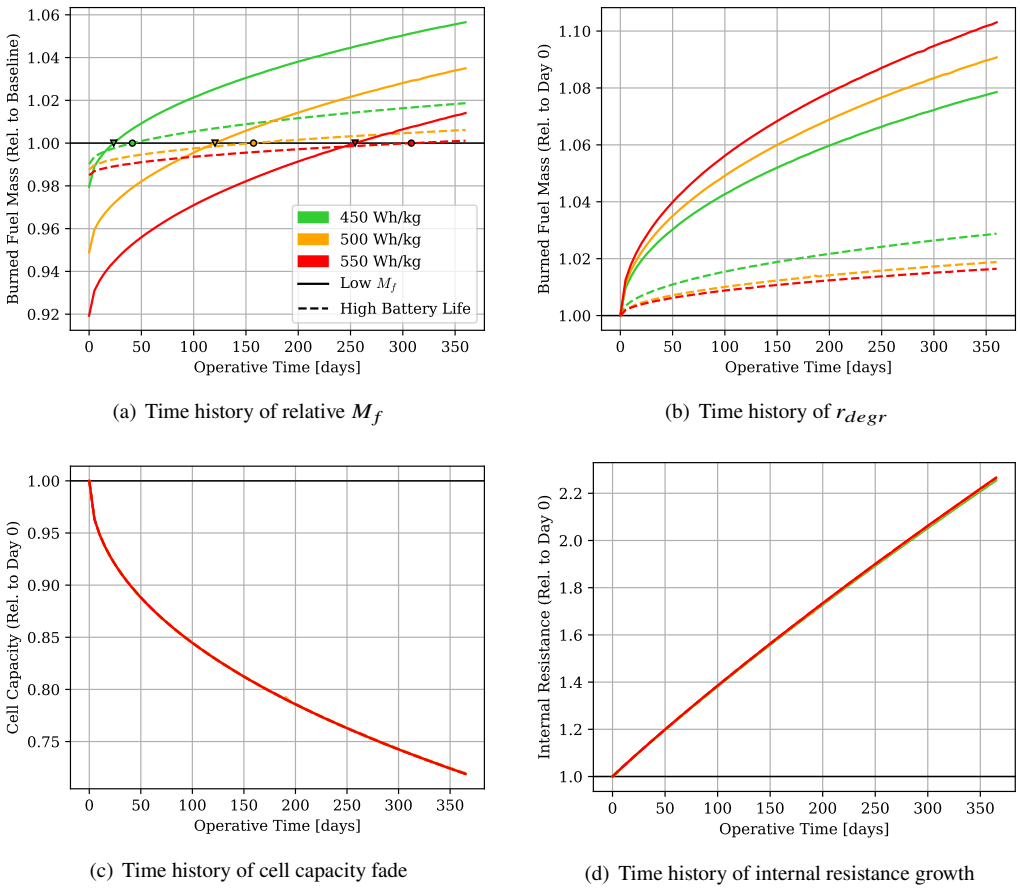

(a) Time history of relative M_f

(b) Time history of r_{degr}

(c) Time history of cell capacity fade

(d) Time history of internal resistance growth

Fig. 10 Degradation histories of extreme points for each $e_{battery}$ case.

Comparing the geometry of the battery packs of these six cases (Table 5) shows that the number of cell modules is correlated with the r_{degr} parameter of Fig. 10(b): the higher this quantity the faster the rate of degradation. While each cell ages at the same rate, the airplane is carrying more weight, and therefore, with less electrical power compensating for the inefficiency of the extra weight, the fuel consumption grows faster as the battery ages. In summary, the effective specific energy of the pack decreases with cell aging, eroding the benefits calculated at day zero, with a leveraging effect caused by the size of the battery pack. Therefore, more specific energy from the start enables the battery to last longer before servicing.

D. Effects of $e_{battery}$ on Aircraft Performance

Figure 11 presents the percentile change in fuel consumption, energy consumption, and take-off mass relative to the baseline. It contains three selections of the Pareto front for each level of battery pack technology. The values refer to the day-zero condition.

All the investigated cases are less efficient than the baseline, requiring more energy to fly the same mission. The specific energy of the fuel is at least 20 times higher than the batteries, increasing the take-off mass when trading one source for the other. Hence, the heavier airplane requires more energy to fly, despite the lower fuel consumption. Indeed,

$e_{battery}$ [Wh/kg]	Pack Life [Days]	r_{degr}	N_{cells}	N_{series}	$N_{modules}$	M_{fuel} [kg]	$M_{battery}$ [kg]	TOM [kg]
450	24	1.0838	44880	136	663	1211.2	5181.8	22943
500	121	1.0957	46784	136	344	1172.6	5248.1	22970
550	271	1.1085	112608	136	828	1136.9	5302.5	22989
450	48	1.0299	32096	136	236	1228.7	1839.8	19618
500	158	1.0197	21080	136	155	1225.7	1085.2	18860
550	310	1.0168	18224	136	134	1222.9	851.9	18624

Table 5 Details of the selected design points for discussion.

when the take-off mass is constrained, the energy consumption decreases as the specific energy increments (Fig. 11(b)). In this situation, the higher efficiency of the electrical power chain compensates for the power required to fly heavier aircraft.

All three conditions present a reduction in fuel consumption when $e_{battery}$ is above 400 Wh/kg. However, the condition with the highest battery life has no linear reduction with specific energy. Instead, it is constant at around 2%, with a reduction in take-off mass. As pointed out in the previous section V.C, this design takes advantage of the increased specific energy for reducing the number of cells in the battery pack, containing the increment of fuel consumption after the battery is aged. This set of points does not correspond to the lowest r_{degr}, however. Minimizing only that objective would entail not including any battery pack at all in the design. The fuel consumption would stay identical as the object causing its increment is missing. (See Fig. 12(d)).

Overall, the Pareto midpoint balances the two extreme cases, with an increment of energy consumption of 7.5%. The three scenarios show that, when the battery technology is fixed, the choice of EMS affects the efficiency of the aircraft, via the increment of battery pack mass. Finally, when the cells age, more fuel will be required, widening the inefficiency in energy consumption.

E. Suggested Energy Management Strategies

From the knowledge obtained in the previous sections, it was found that the average value of DOH for each segment is correlated with the energy density of the battery and the amount of maximum take-off mass. More DOH is allocated in the climb segment than the cruise segment, while the slope is increasing in cruise and is ambiguous for climb. Because in this study the battery pack is sized to match the EMS at day zero, the average value of DOH drives the increment of fuel consumption as the battery ages through the mechanism of dead weight.

Figure 12 presents the EMS of the three scenarios analyzed in the previous section plus the EMS with the least r_{degr}. They present the trends described so far, showing no clear preference for the slope of the DOH function in climb. Higher $e_{battery}$ allows higher average DOH across the mission when fuel consumption is the priority (Fig. 12(b)). In contrast, when battery life is maximized, the higher energy density is used for reducing the amount of battery mass through a reduction of DOH (Fig. 12(c)). As pointed out previously, this condition does not correspond to the EMS of minimum degradation. Instead, minimum r_{degr} is obtained when no hybridization is used (Fig. 12(d)). While in practice is an undesirable result, it further exhibits the relation between the battery mass and the increment of fuel consumption as the battery pack ages: no increment is present if no batteries are used.

In summary, the presented EMS should be used as a general recommendation considering the identified interactions between pack energy density, battery aging, and environmental requirements. They are limited by the selected design mission, the aircraft design selected as the starting point, and the figures of merit selected for the analysis. Consequently, designers should perform their optimization study for their specific application and use the presented results as a sanity check.

F. Probability of achieving the expected technological requirements

The discussion presented so far underlined the importance of $e_{battery}$ for the feasibility of the scenarios presented in this study and hybrid-electric propulsion. However, most studies do not quantify the uncertainty of their timelines, instead, they assume a year far in the future to justify their assumption. In this last section, the probability of technological availability is estimated with a regression analysis of current and expected specific cell energy densities. The intention

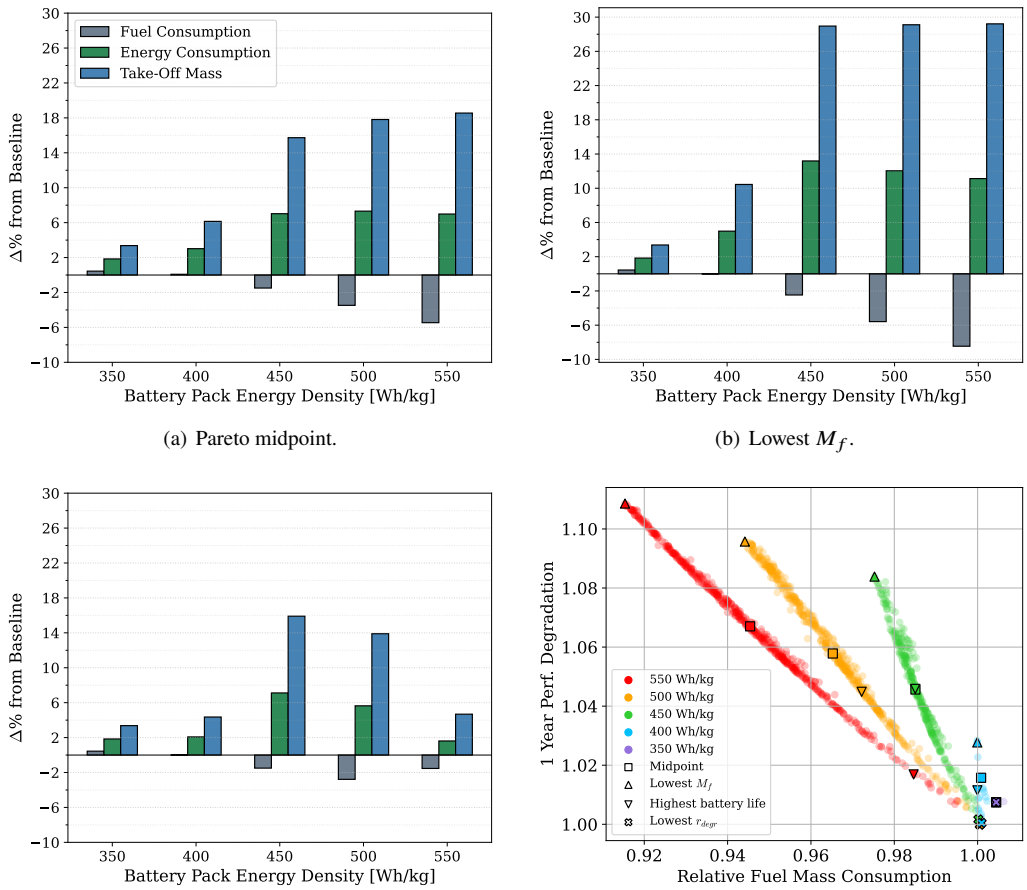

(a) Pareto midpoint.

(b) Lowest M_f.

(c) Highest battery pack life.

(d) Position of points on the Pareto front.

Fig. 11 Aircraft performance at representative points in the Pareto front.

is to quantify when it is reasonable to expect the required $e_{battery}$ values to be given the history of cell technology development.

Data has been extracted from the Battery 2030+ Roadmap report [37] from the year 2010 onwards. Two scenarios are presented, one conservative and one optimistic. The first assumes the cell energy density will improve linearly in time (Fig. 13(a)). The second scenario assumes it will improve exponentially (Fig. 13(b)). Ordinary Least Squares (OLS) have been used to construct the regression models using standard procedures. Both models have satisfying correlation ($R^2 = 0.83$ and $R^2 = 0.78$ respectively) and good modeling (P-values of the F test are smaller than 1^{-10} in both cases).

The energy density of the battery packs is lower than the cell one due to the inert mass added by the cooling system, packaging, and control electronics. The pack-to-cell mass ratio of this study is 1.5 (Table 2). By applying this technological assumption to the statistical prediction of future cell technology, it is possible to estimate the probability of obtaining a battery pack with at least the specified energy density. Figures 13(c) and 13(d) present these results for the values of $e_{battery}$ which could match or improve over the baseline.

The two scenarios are considerably different. Under the conservative scenario, the year 2040 is the earliest date where a battery pack of 400 Wh/kg is expected to be available with 55% confidence. Conversely, the optimistic scenario estimates the year 2034 for the same value and confidence. This difference is more pronounced for higher energy densities. In the conservative scenario, in the year 2050 there is a 60% chance a battery pack with 500 Wh/kg is available, while the year 2038 is indicated in the optimistic scenario. The full range of predictions for each level of battery pack energy density are presented in Table 6.

As has been noted, the assumption of the future trend leads to different conclusions on the feasibility of hybrid-electric

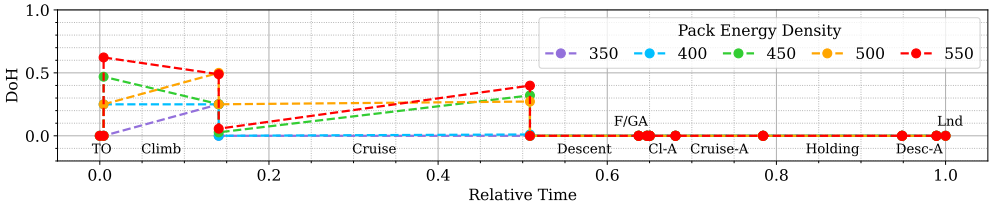

(a) Pareto midpoint.

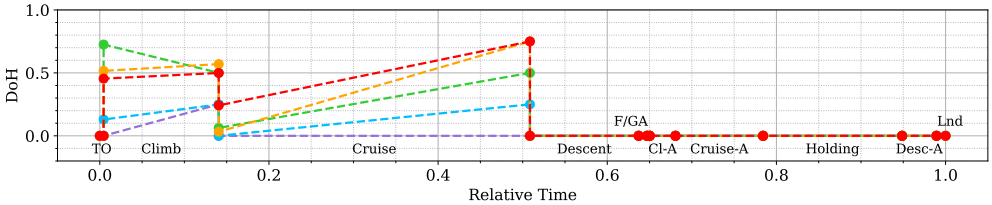

(b) Lowest M_f.

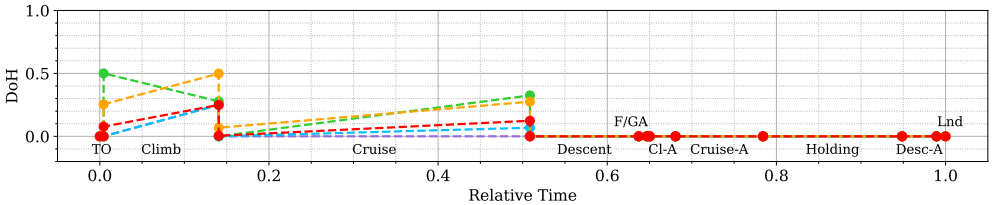

(c) Longest battery life

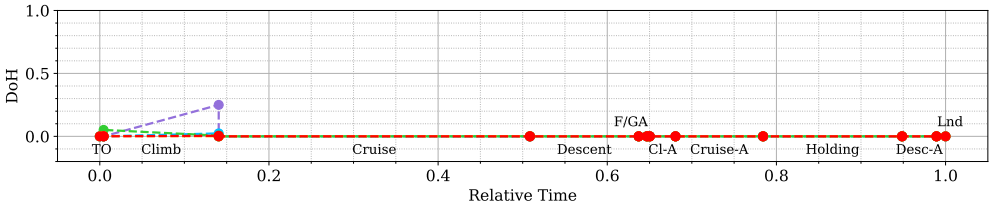

(d) Lowest r_{degr}.

Fig. 12 EMS of the three scenarios analyzed in Section V.D, compared to the lowest r_{degr} EMS.

$e_{battery}$ [Wh/kg]	Conservative scenario	Optimistic scenario
400	2040-2043	2034-2038
450	2044-2048	2035-2040
500	2049-2053	2038-2042
550	2053-2058	2039-2044

Table 6 Predicted years of technological availability, years corresponding to the 50%-90% probabilities respectively.

aircraft. While the conservative scenario is the most likely, the automotive and renewable sectors have been heavily investing in the development of the technology, which could accelerate the rate of development. On a final note, this analysis is conditioned by the assumption of the pack-to-cell mass ratio. As pointed out in section III.C, this parameter is affected by the safety and certification requirements. Increasing or decreasing it would increase or decrease the probability of availability. If it would be expected to decrease in the future, the required enabling technology could

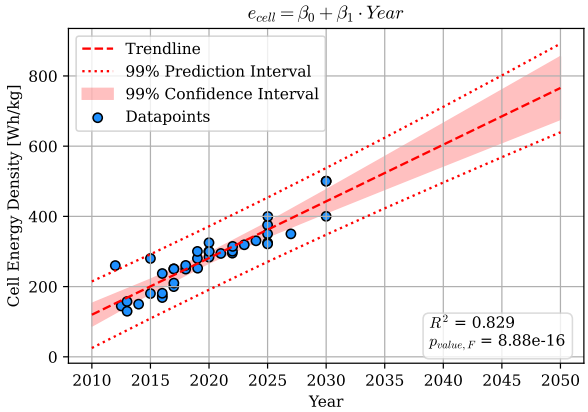

(a) Conservative trendline of Cell energy density.

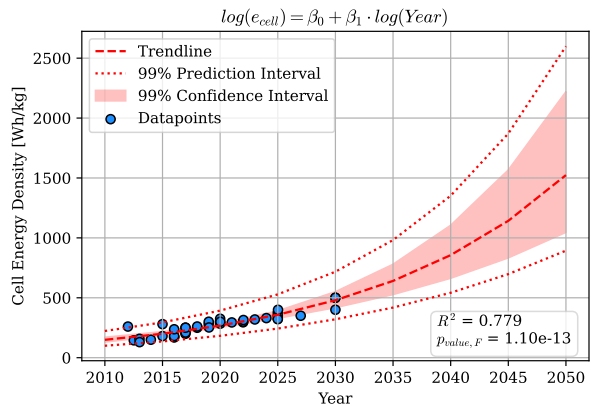

(b) Optimistic trendline of Cell energy density.

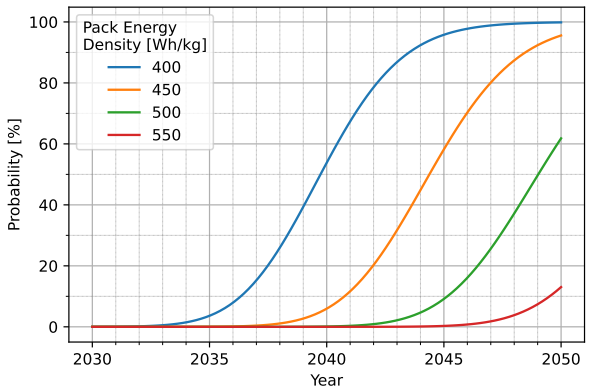

(c) Probability of availability of a battery pack with at least the required specific energy, conservative scenario. (Pack-to-Cell Mass ratio of 1.5).

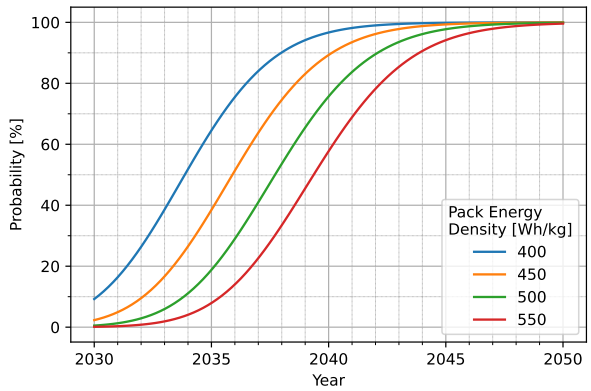

(d) Probability of availability of a battery pack with at least the required specific energy, optimistic scenario. (Pack-to-Cell Mass ratio of 1.5).

Fig. 13 Statistical modeling of future battery technology.

materialize sooner than predicted in this section.

VI. Conclusions

In this work, the interaction between the battery energy density and energy management strategy on the aging of the battery pack, the fuel consumption, and environmental compatibility was analyzed. The application of a probabilistic design space exploration framework generated data that shed light on the optimal power schedule and the minimal technological requirements.

The specific energy of the batteries was identified as a key driver in the achievable reduction of fuel consumption and emissions, setting the maximum amount of achievable DOH in the EMS. This parameter affects the life of the battery pack, increasing its effective use before the fuel consumption of the airplane is identical to the baseline. Finally, 400 Wh/kg was identified as the minimum specific energy required to improve the baseline emissions. This translates into a requirement of cells with 600 Wh/kg specific energy, expected to be available between the years 2034-2040, depending on the technological scenario. Battery packs with higher specific energy, required to make hybrid-electric propulsion feasible, are predicted to be available in the time window 2038-2050. However, this prediction is conditioned by the current trend of technological improvement and a fixed 1.5 pack-to-cell mass weight ratio. On a final note, every design, regardless of the specific energy, is less efficient from the baseline, despite reducing the fuel consumption. This is a required compromise for pushing towards sustainable aviation since no battery technology can achieve a 1:1 ratio of specific energy with aviation fuel.

The inclusion of cell aging to the battery model introduced additional considerations in the definition of the EMS.

While striving for the highest DOH possible is beneficial for the immediate reduction of emissions, it shortens the operational life of the battery pack. The mechanism of this phenomenon was identified not in the aging rate of the cells, which was identical in every case studied, but in the number of batteries employed in each specific case. Indeed, as the batteries aged, the effective energy density of the pack decreased, requiring the aircraft to consume more fuel. This effect is stronger the heavier the battery pack. Hence, when attempting to minimize the effects of degradation, the optimizer identified designs with the least amount of cells, taking advantage of the higher energy density when possible. As a result, the EMS should be moderated to avoid quickly degrading the zero-day performance.

VII. Future Work

The knowledge obtained in this study is limited to a single mission. It is suggested to extend it by introducing different operating missions, which would produce more insights into the trade-off between battery aging and the reduction of fuel consumption and emissions. This would be of interest to airline operators employing hybrid-electric aircraft, minimizing direct operating costs and programming maintenance. On this last note, the study could be extended by including also a gas turbine lifing model for identifying ideal operating conditions where battery pack maintenance and gas turbine maintenance would be required, minimizing aircraft downtime.

Another extension is introducing operating conditions that would affect cell aging directly. The scenario presented in this paper assumed a full discharge and recharge of the battery pack after each flight. However, partial re-charging and discharging is necessary for high-volume operations and fast turnaround of the aircraft [36]. This would introduce stresses that would affect the health of the cells directly. Finally, the constant cell temperature assumption could be relaxed with the introduction of a seasonal effect or a thermal management system cooling model [38].

From the perspective of design, further developments will extend this work by incorporating other technological factors, such as the battery pack-to-cell ratio and the thermal operational limits. These parameters would come into play in the estimation of the technological availability of the analyzed scenarios. In particular, the pack-to-cell ratio, if expected to improve in the next years, would reduce the time to the introduction of hybrid-electric regional aircraft.

Acknowledgments

This project has received funding from the European Union's Horizon 2020 Research and Innovation program under Grant Agreement No 875551. A. Spinelli thanks Dr. Bahareh Zaghari and Tianzhi Zhou for their assistance in the development of the battery pack model. He thanks Dr. Evangelia Pontika for her help in the mission analysis modeling. He also thanks Dr. Hossein B. Enalou for his expertise in the gas turbine model. Finally, he thanks Dr. Boris Berseneff from Université Grenoble Alpes for his expertise in energy storage technology and for providing the historic data on cells.

References

[1] Bowman, C. L., Felder, J. L., and Marien, T., "Turbo-and Hybrid-Electrified Aircraft Propulsion Concepts for Commercial Transport," *2018 AIAA/IEEE Electric Aircraft Technologies Symposium (EATS)*, 2018, pp. 1–8. https://doi.org/10.2514/6.2018-4984.

[2] Xie, Y., Savvarsial, A., Tsourdos, A., Zhang, D., and Gu, J., "Review of hybrid electric powered aircraft, its conceptual design and energy management methodologies," *Chinese Journal of Aeronautics*, Vol. 34, No. 4, 2021, pp. 432–450. https://doi.org/10.1016/j.cja.2020.07.017.

[3] Riboldi, C. E., "Energy-optimal off-design power management for hybrid-electric aircraft," *Aerospace Science and Technology*, Vol. 95, 2019, p. 105507. https://doi.org/https://doi.org/10.1016/j.ast.2019.105507.

[4] Pinto Leite, J. P. S., and Voskuijl, M., "Optimal energy management for hybrid-electric aircraft," *Aircraft Engineering and Aerospace Technology*, Vol. 92, No. 6, 2020, p. 851 – 861. https://doi.org/10.1108/AEAT-03-2019-0046.

[5] Donateo, T., and Ficarella, A., "A modeling approach for the effect of battery aging on the performance of a hybrid electric rotorcraft for urban air-mobility," *Aerospace*, Vol. 7, No. 5, 2020. https://doi.org/10.3390/AEROSPACE7050056.

[6] Clarke, M. A., and Alonso, J. J., "Forecasting the Operational Lifetime of Electric Aircraft Through Battery Degradation Modeling," *AIAA SciTech 2022 Forum*, AIAA, San Diego, CA, 2022. https://doi.org/10.2514/6.2022-1996.

[7] "FutPrInt50: Collaborating towards sustainable regional aviation," *European Energy Innovation*, Vol. 1, 2022, p. 12. URL https://www.europeanenergyinnovation.eu/OnlinePublication/Spring2022/index.html#p=13.

[8] Moebs, N., Eisenhut, D., Windels, E., van der Pols, J., and Strohmayer, A., "Adaptive Initial Sizing Method and Safety Assessment for Hybrid-Electric Regional Aircraft," *Aerospace*, Vol. 9, No. 3, 2022. https://doi.org/10.3390/aerospace9030150.

[9] Candeloro, P., Martellini, E., Nederlof, R., Sinnige, T., and Pagliaroli, T., "An Experimental Study of the Aeroacoustic Properties of a Propeller in Energy Harvesting Configuration," *Fluids*, Vol. 7, No. 7, 2022. https://doi.org/10.3390/fluids7070217.

[10] Kiran, A., Zaghari, B., Sinnige, T., Pontika, E., Enalou, H. B., Kipouros, T., and Laskaridis, P., "The Impact of Electric Machine and Propeller Coupling Design on Electrified Aircraft Noise and Performance," *AIAA SciTech 2023 Forum*, AIAA, National Harbor, MD, 2023.

[11] Liu, X., Furrer, D., Kosters, J., and Holmes, J., "Vision 2040 : A Roadmap for Integrated, Multiscale Modeling and Simulation of Materials and Systems," Nasa/cr—2018-219771, 2018. URL https://ntrs.nasa.gov/citations/20180002010.

[12] Pornet, C., Gologan, C., Vratny, P. C., Seitz, A., Schmitz, O., Isikveren, A. T., and Hornung, M., "Methodology for sizing and performance assessment of hybrid energy aircraft," *Journal of Aircraft*, Vol. 52, No. 1, 2015, pp. 341–352. https://doi.org/10.2514/1.C032716.

[13] Zamboni, J., Vos, R., Emeneth, M., and Schneegans, A., "A method for the conceptual design of hybrid electric aircraft," *AIAA Scitech 2019 Forum*, 2019, p. 1587. https://doi.org/10.2514/6.2019-1587.

[14] Riboldi, C. E., "An optimal approach to the preliminary design of small hybrid-electric aircraft," *Aerospace Science and Technology*, Vol. 81, 2018, pp. 14–31. https://doi.org/10.1016/j.ast.2018.07.042.

[15] Bianchi, D., Amadori, K., Bäckström, E., Jouannet, C., and Secco, N., "An Uncertainty-based Framework for Technology Portfolio Selection for Future Aircraft Program," *AIAA Scitech 2021 Forum*, 2021, p. 1479. https://doi.org/10.2514/6.2021-1479.

[16] Guenov, M. D., Chen, X., Molina-Cristóbal, A., Riaz, A., van Heerden, A. S., and Padulo, M., "Margin allocation and tradeoff in complex systems design and optimization," *AIAA journal*, Vol. 56, No. 7, 2018, pp. 2887–2902. https://doi.org/10.2514/1.J056357.

[17] Spinelli, A., Enalou, H. B., Zaghari, B., Kipouros, T., and Laskaridis, P., "Application of Probabilistic Set-Based Design Exploration on the Energy Management of a Hybrid-Electric Aircraft," *Aerospace*, Vol. 9, No. 3, 2022, p. 147. https://doi.org/10.3390/aerospace9030147.

[18] Martins, J. R., and Lambe, A. B., "Multidisciplinary design optimization: a survey of architectures," *AIAA Journal*, Vol. 51, No. 9, 2013, pp. 2049–2075. https://doi.org/10.2514/1.J051895.

[19] Singer, D. J., Doerry, N., and Buckley, M. E., "What is set-based design?" *Naval Engineers Journal*, Vol. 121, No. 4, 2009, pp. 31–43. https://doi.org/10.1111/j.1559-3584.2009.00226.x.

[20] Blanchard, B. S., Fabrycky, W. J., and Fabrycky, W. J., *Systems engineering and analysis*, Vol. 4, Prentice hall Englewood Cliffs, NJ, 1990.

[21] Georgiades, A., Sharma, S., Kipouros, T., and Savill, M., "ADOPT: An augmented set-based design framework with optimisation," *Design Science*, Vol. 5, 2019. https://doi.org/10.1017/dsj.2019.1.

[22] Spinelli, A., Anderson, L., Enalou, H. B., Zaghari, B., Kipouros, T., and Laskaridis, P., "Application of Probabilistic principles to Set-Based Design for the optimisation of a hybrid-electric propulsion system," *IOP Conference Series: Materials Science and Engineering*, Vol. 1226, IOP Publishing, 2022, p. 012064. https://doi.org/10.1088/1757-899X/1226/1/012064.

[23] Cano, T. C., Castro, I., Rodriguez, A., Lamar, D. G., Khalil, Y. F., Albiol-Tendillo, L., and Kshirsagar, P., "Future of electrical aircraft energy power systems: An architecture review," *IEEE Transactions on Transportation Electrification*, Vol. 7, No. 3, 2021, pp. 1915–1929. https://doi.org/10.1109/TTE.2021.3052106.

[24] Hüllermeier, E., and Waegeman, W., "Aleatoric and epistemic uncertainty in machine learning: An introduction to concepts and methods," *Machine Learning*, Vol. 110, No. 3, 2021, pp. 457–506.

[25] Kipouros, T., Inselberg, A., Parks, G., and Savill, A. M., "Parallel coordinates in computational engineering design," *54th AIAA/ASME/ASCE/AHS/ASC Structures, Structural Dynamics, and Materials Conference*, 2013, p. 1750. https://doi.org/10.2514/6.2013-1750.

[26] ATR, "ATR-72-600 Factsheet," , 2022. URL https://www.atr-aircraft.com/wp-content/uploads/2020/07/Factsheets_-_ATR_72-600.pdf.

[27] Jackson, P., Peacock, L., Bushell, S., Willis, D., and Winchester, J., *Jane's All the Worlds Aircraft: Development and Production. 2018-2019*, IHS Markit, 2018.

[28] MacMillan, W., "Development of a modular-type computer program for the calculation of gas turbine off-design performance," Ph.D. thesis, Cranfield University, Cranfield UK, 1974.

[29] Nkoi, B., Pilidis, P., and Nikolaidis, T., "Performance of small-scale aero-derivative industrial gas turbines derived from helicopter engines," *Propulsion and Power Research*, Vol. 2, No. 4, 2013, pp. 243–253. https://doi.org/10.1016/j.jppr.2013.11.001.

[30] DuBois, D., and Paynter, G. C., ""Fuel Flow Method2" for Estimating Aircraft Emissions," *Non-Conference Specific Technical Papers - 2006*, SAE International, 2006. https://doi.org/https://doi.org/10.4271/2006-01-1987.

[31] Filippone, A., and Bojdo, N., "Statistical model for gas turbine engines exhaust emissions," *Transportation Research Part D: Transport and Environment*, Vol. 59, 2018, pp. 451–463. https://doi.org/https://doi.org/10.1016/j.trd.2018.01.019.

[32] Ceraolo, M., Lutzemberger, G., and Huria, T., "Experimentally-Determined Models for High-Power Lithium Batteries," *SAE 2011 World Congress & Exhibition*, SAE International, 2011. https://doi.org/10.4271/2011-01-1365.

[33] Chin, J., Schnulo, S. L., Miller, T., Prokopius, K., and Gray, J. S., "Battery Performance Modeling on SCEPTOR X-57 Subject to Thermal and Transient Considerations," *AIAA Scitech 2019 Forum*, 2019. https://doi.org/10.2514/6.2019-0784.

[34] Chin, J. C., Look, K., McNichols, E. O., Hall, D. L., Gray, J. S., and Schnulo, S. L., "Battery Cell-to-Pack Scaling Trends for Electric Aircraft," *2021 AIAA/IEEE Electric Aircraft Technologies Symposium (EATS)*, 2021, pp. 1–15. https://doi.org/10.23919/EATS52162.2021.9704819.

[35] Schmalstieg, J., Käbitz, S., Ecker, M., and Sauer, D. U., "A holistic aging model for Li (NiMnCo) O2 based 18650 lithium-ion batteries," *Journal of Power Sources*, Vol. 257, 2014, pp. 325–334. https://doi.org/10.1016/j.jpowsour.2014.02.012.

[36] Spinelli, A., Krupa, G. P., Kipouros, T., Berseneff, B., and Bui Van, A.-L., "Investigation of the operational flexibility of a regional hybrid-electric aircraft," *Journal of Physics: Conference Series*, IOP Publishing, 2023. Submitted for publication.

[37] Edström, K., Ayerbe, E., Cekic-Laskovic, I., Dominko, R., Fichtner, M., Grimaud, A., Kumberg, J., Perraud, S., Punckt, C., and Vegge, T., "Battery 2030+: Inventing the sustainable batteries of the future. Research Needs and Future Actions," Battery 2030+ roadmap, 2022. URL https://battery2030.eu/wp-content/uploads/2022/07/BATTERY-2030-Roadmap_Revision_FINAL.pdf.

[38] Gkoutzamanis, V. G., Tsentis, S. E., Valsamis Mylonas, O. S., Kalfas, A. I., Kyprianidis, K. G., Tsirikoglou, P., and Sielemann, M., "Thermal Management System Considerations for a Hybrid-Electric Commuter Aircraft," *Journal of Thermophysics and Heat Transfer*, Vol. 36, No. 3, 2022, pp. 650–666. https://doi.org/10.2514/1.T6433.

Cranfield University

CERES Research Repository **https://dspace.lib.cranfield.ac.uk/**

School of Aerospace, Transport and Manufacturing (SATM) Staff publications (SATM)

Set-based design space exploration to investigate the effect of energy storage durability on the energy management strategy of a hybrid-electric aircraft

Spinelli, Andrea

2023-01-19

Attribution-NonCommercial 4.0 International

Spinelli A, Krupa GP & Kipouros T (2023) Set-based design space exploration to investigate the effect of energy storage durability on the energy management strategy of a hybrid-electric aircraft. In: AIAA SciTech Forum 2023, 23-27 January 2023, National Harbor, Maryland
https://doi.org/10.2514/6.2023-0837

Downloaded from CERES Research Repository, Cranfield University